Wavelet Expansion and High-order Regularization for Multiscale Fluid-motion Estimation

Pierre Dérian, Patrick Héas, Cédric Herzet, Etienne Mémin

INRIA

INSTITUT NATIONAL DE RECHERCHE EN INFORMATIQUE ET EN AUTOMATIQUE

Wavelet Expansion and High-order Regularization for Multiscale Fluid-motion Estimation

Pierre Dérian — Patrick Héas — Cédric Herzet — Étienne Mémin

N° 7348 — version 2

initial version July 2010 — revised version Juillet 2010

Observation and Modeling for Environmental Sciences

ISSN 0249-6399 ISRN INRIA/RR--7348--FR+ENG

INSTITUT NATIONAL
DE RECHERCHE
EN INFORMATIQUE
ET EN AUTOMATIQUE

INRIA

centre de recherche
RENNES - BRETAGNE ATLANTIQUE

Wavelet Expansion and High-order Regularization for Multiscale Fluid-motion Estimation

Pierre Dérian , Patrick Héas , Cédric Herzet , Étienne Mémin

Theme : Observation and Modeling for Environmental Sciences
Équipe-Projet Fluminance

Rapport de recherche n° 7348 — version 2* — initial version July 2010 — revised version Juillet 2010 — 19 pages

Abstract: We consider a novel optic flow estimation algorithm based on a wavelet expansion of the velocity field. In particular, we propose an efficient gradient-based estimation algorithm which naturally encompasses the estimation process into a multiresolution framework while avoiding most of the drawbacks common to this kind of hierarchical methods. We then emphasize that the proposed methodology is well-suited to the practical implementation of high-order regularizations. The powerfulness of the proposed algorithm and regularization schemes are finally assessed by simulation results on challenging image sequences of turbulent fluids.

Key-words: optic flow, wavelets, motion regularity, fluid flows, turbulence

* INRIA report number has been corrected.

Centre de recherche INRIA Rennes – Bretagne Atlantique
IRISA, Campus universitaire de Beaulieu, 35042 Rennes Cedex
Téléphone : +33 2 99 84 71 00 — Télécopie : +33 2 99 84 71 71

Formulation en ondelettes et régularisation d'ordre élevé pour l'estimation multi-échelles de mouvements de fluides.

Résumé : Un algorithme original d'estimation du flux optique est introduit, basé sur une décomposition en ondelettes du champ de vitesse. Cet algorithme inscrit le processus d'estimation dans un cadre multirésolution, en évitant la plupart des écueils qui accompagnent généralement ce type d'approches séquentielles. Cette approche permet en outre l'implémentation aisée de régularisations d'ordre élevé. Les performances de l'algorithme d'estimation et des régularisations introduits sont évaluées sur des séquences d'images de fluides turbulents.

Mots-clés : flux optique, ondelettes, estimation de mouvement, fluide, turbulence

1 Introduction

Optic flow estimation consists in recovering the apparent motion of a scene through spatial and temporal variations of an image intensity. This estimation process usually requires to solve complex *non-linear* and *underdetermined* inverse problems. Therefore, since the seminal work of Horn and Schunck [6], numerous approaches have been proposed to address these issues.

A standard procedure to deal with the non-linear nature of the problem is to resort to multiresolution strategies [2]. These approaches consist in solving the optic flow estimation problem by considering a sequence of coarse-to-fine linearized sub-problems. Although leading to good empirical results, this technique has nevertheless a number of drawbacks. First, the estimates computed at coarse levels can never be re-evaluated at finer scales. Moreover, the sub-problems considered at each level follow from a "ad-hoc" filtering of the image sequence. In particular, there is usually no obvious connections between the data processed at each level. Finally, standard multiresolution techniques rely on linear approximation of the initial problem. Now, the validity of such approximation can be limited in case of large displacements.

The undertermined nature of the optic flow estimation problem is usually referred to as *"aperture problem"*. Resolving the underdetermination imposes to add some prior information about the sought motion field. In many contributions dealing with rigid-motion estimation, first-order regularization (enforcing the spatial gradient of the velocity to be weak) is considered with success. However, when tackling more challenging problems such as motion estimation of turbulent fluids, this simple prior turns out to be inadequate. Instead, higher-order regularizers allowing to enforce physically-sound constraints have to be considered [4, 12, 5]. Unfortunately, current implementations of such regularizers suffer from instabilities and turn out to be a difficult problem.

In this paper, we propose an optic flow estimation procedure based on a wavelet expansion of the velocity field. This approach turns out to offer a nice mathematical framework for multiresolution estimation algorithms. In particular, we emphasize that estimating wavelet coefficients in a sequential way reduces to a multiresolution estimation algorithm which avoids the common drawbacks mentioned above. We propose an efficient implementation of the corresponding optic flow estimation problem whose complexity scales linearly with the problem dimensions. Note that another algorithm based on wavelet expansion has been previously proposed in [11]. However, unlike the algorithm presented hereafter, its complexity is of intractable polynomial order.

Moreover, we consider the effective implementation of high-order regularization schemes. In particular, we emphasize that enforcing high-order regularization on the velocity field is equivalent to imposing very simple constraints on the wavelet coefficients at proper scales. Based on this observation, we elaborate three possible implementations of high-order regularization scheme and assess their relevance on challenging image sequence of turbulent fluid motions. Simulation results prove that the proposed approach outperforms the most effective state-of-the-art algorithms while having a lower complexity order.

2 Introduction to optic flow

2.1 Aperture problem

Optic flow estimation is a well-known difficult ill-posed inverse problem. It consists in estimating the apparent motion of a 3D scene through image intensity $I(\mathbf{x},t)$ variations in space $\mathbf{x}=(x_1,x_2)\in\Omega\subset\mathbb{R}^2$ and time $t\in\mathbb{R}$. The optic flow, identified by a 2D velocity field $\mathbf{v}(\mathbf{x},t):\Omega\times\mathbb{R}^+\mapsto\mathbb{R}^2$ is the projection on the image plane of the 3D scene velocity. Under rigid motion and stable lighting conditions, $\mathbf{v}=(u,v)^T$ satisfies the standard Displaced Frame Difference (DFD) equation. Let us denote by $I_0(\mathbf{x})$ and $I_1(\mathbf{x})$ two consecutive image samples of the continuous sequence $I(\mathbf{x},t)$ which has been discretized in time with a unit interval. The DFD equation reads:

$$f_d(I,\mathbf{v})=I_1(\mathbf{x}+\mathbf{v}(\mathbf{x}))-I_0(\mathbf{x})=0. \tag{1}$$

A linearized version of model (1), so-called the motion compensate Optic Flow Constraint (OFC) equation, is obtained by linearization of I_1 around $\mathbf{x}+\tilde{\mathbf{v}}(\mathbf{x})$[1]:

$$\tilde{f}_d(I,\mathbf{v})=I_1(\mathbf{x}+\tilde{\mathbf{v}}(\mathbf{x}))-I_0(\mathbf{x})+\nabla I_1(\mathbf{x}+\tilde{\mathbf{v}}(\mathbf{x}))\cdot\mathbf{v}'=0. \tag{2}$$

where $\mathbf{v}'=\mathbf{v}-\tilde{\mathbf{v}}$.

For other configurations, many other brightness evolution models have been proposed in the literature to link the image intensity function to the sought velocity fields [8]. In the sequel, we will sometimes use the generic notation $\mathcal{M}(I,\mathbf{v})$ to denote the model linking images and their underlying velocity field.

However, all these evolution models remain underconstrained, as they provide for each time t only one equation for two unknowns (u,v) at each spatial location $\mathbf{x}=(\mathrm{x}_1,\mathrm{x}_2)^T$. To deal with this underconstrained estimation problem, so called aperture problem, the most common setting consists in enforcing some spatial coherence to the solution.

2.2 Regularization schemes

This coherence is imposed either: *i) explicitly*, by constraining the motion field to be of the form $\mathbf{v}=\Phi(\mathbf{\Theta})$, where Φ is function parameterized by $\mathbf{\Theta}$ (piecewise polynomial functions are often used); *ii) globally*, through a regularization functional defined over the whole image domain. We briefly describe these two approaches hereafter.

Explicit regularization schemes penalize discrepancies from model (1) by minimizing an "energy" with respect to $\mathbf{\Theta}$, *i.e.*

$$\hat{\mathbf{v}}=\Phi\Big(\arg\min_{\mathbf{\Theta}} J_{obs}(I,\Phi(\mathbf{\Theta}))\Big), \tag{3}$$

where

$$J_{obs}(I,\Phi(\mathbf{\Theta}))=\frac{1}{2}\int_\Omega\left[\mathcal{M}(I,\Phi(\mathbf{\Theta}))\right]^2 d\mathbf{x}. \tag{4}$$

If model $\mathcal{M}$ is linear, motion estimate $\hat{\mathbf{v}}$ is simply obtained by solving a low-dimensional system of linear equations. Alternatively to quadratic penalization, robust functions (so-called M-estimators) can be used to penalize model

[1] The current motion estimate is usually used to define $\tilde{\mathbf{v}}(\mathbf{x})$.

discrepancies. This yields to semi-quadratic functionals which preserve locally convex properties [3]. For clarity of the presentation, we will however restrict ourselves to quadratic penalty functions in the following.

Global regularization schemes in their simplest form define the estimation problem through the minimization of a functional composed of two terms balanced by a regularization coefficient $\gamma > 0$:

$$J(I, \mathbf{v}, \gamma) = J_{obs}(I, \mathbf{v}) + \gamma J_{reg}(\mathbf{v}). \tag{5}$$

Thus, motion estimate $\hat{\mathbf{v}}$ satisfies $\hat{\mathbf{v}} = \arg\min_{\mathbf{v}} J(\mathbf{v}, I, \gamma)$. The first term, J_{obs} (the "data term") is defined by (4) with $\mathbf{v} = \Phi(\boldsymbol{\Theta}) = \boldsymbol{\Theta}$. The second term, J_{reg} (the "regularization term"), encourages the solution to follow some prior smoothness model formalized with function f_r:

$$J_{reg}(\mathbf{v}) \quad = \quad \frac{1}{2}\int_{\Omega} |f_r(u, \mathbf{x})|^2 + |f_r(v, \mathbf{x})|^2 d\mathbf{x} \tag{6}$$

where $|.|^2$ denotes the $\mathcal{L}^2$ norm. An n-order regularization writes in its simplest form:

$$f_r(u, \mathbf{x}) = \frac{\partial^n u(\mathbf{x})}{\partial \mathbf{x}^n}, \; f_r(v, \mathbf{x}) = \frac{\partial^n v(\mathbf{x})}{\partial \mathbf{x}^n}. \tag{7}$$

A first-order regularizer (*i.e.* n=1) enforcing weak spatial gradients of the two components u and v of the velocity field $\mathbf{v}$ is very often used [6]. Higher-order regularizers (*i.e.* $n > 1$) have been proposed in the literature in the case of fluid flows [4, 12]. However, since motion variables are considered on the pixel grid, an approximation of continuous spatial derivatives by discrete operators is required. For regular pixel grids, it is usually done using finite difference schemes. Nevertheless, it is well known that ensuring stability of the discretization schemes of high-order regularizer constitutes a difficult problem.

2.3 Common multiresolution strategy

A major problem with differential models such as (2) is the estimation of velocities for large displacements in the images. Indeed, the equations for the inversion are only valid if the solution remains in the region of linearity of the image intensity function. A standard approach for tackling non-linearity is to rely on a multiresolution strategy [2]. This approach consists in choosing some sufficiently coarse resolution in order to make the linearity assumption valid, and to estimate a first displacement field with a low-pass version of the original images. Then, a so-called Gauss-Newton strategy is used by applying successive linearizations around current estimate and warping a multiresolution representation of the images accordingly.

More explicitly, let us introduce the following incremental decomposition of the displacement field at scale 2^j:

$$\mathbf{v}_j = \tilde{\mathbf{v}}_j + \mathbf{v}'_j, \tag{8}$$

where the field $\mathbf{v}'_j$ represents the unknown incremental displacement field at scale 2^j and $\tilde{\mathbf{v}}_j \triangleq \sum_{i<j} \mathcal{P}_j(\mathbf{v}'_i)$ is a coarse motion estimate computed at the previous scales; $\mathcal{P}_j(\mathbf{v}'_i)$ denotes a projection operator which projects $\mathbf{v}'_i$ onto the grid considered at scale 2^j. In order to respect the Shannon sampling theorem,

the coarse scale data term is derived by a low-pass filtering with a kernel[2] $\mathcal{G}_j$ of the original images following by sub-sampling at period 2^j. Using (8), the coarse scale image $I_j(\mathbf{x})$ and the motion-compensated image $\tilde{I}_j(\mathbf{x})$ are then defined as:

$$\left\{ \begin{array}{l} I_j(\mathbf{x}) = \downarrow_{2^j} \circ (\mathcal{G}_j \star I_0(\mathbf{x})) \\ \tilde{I}_j(\mathbf{x}) = \downarrow_{2^j} \circ (\mathcal{G}_j \star I_1(\mathbf{x} + \tilde{\mathbf{v}}_j(\mathbf{x}))) \,, \end{array} \right. \tag{9}$$

where $\downarrow_{2^j}$ denotes an operator sub-sampling the filter output with a period 2^j. It yields a functional J^j_{obs} defined as a linearized version of (1) around $\tilde{\mathbf{v}}_j(\mathbf{x})$:

$$J^j_{obs}(I_j, \mathbf{v}', \mathbf{v}'_{j-1}, ..., \mathbf{v}'_C) = \frac{1}{2} \int_{\Omega_j} \left[\tilde{I}_j(\mathbf{x}) - I_j(\mathbf{x}) + \mathbf{v}'(\mathbf{x}) \cdot \nabla \tilde{I}_j(\mathbf{x}) \right]^2 d\mathbf{x}. \tag{10}$$

Finally, the sought motion estimate $\hat{\mathbf{v}} = \mathbf{v}'_F + \tilde{\mathbf{v}}_F = \mathbf{v}'_F + \sum_{i<F} \mathcal{P}_F(\mathbf{v}'_i)$ is given by solving a system of coupled equations associated to scales $s \in [2^C, 2^F]$:

$$\left\{ \begin{array}{l} \mathbf{v}'_C = \arg\min_{\mathbf{v}'} J^C_{obs}(I_C, \mathbf{v}') \\ . \\ \mathbf{v}'_j = \arg\min_{\mathbf{v}'} J^j_{obs}(I_j, \mathbf{v}', \mathbf{v}'_{j-1}, ..., \mathbf{v}'_C) \\ . \\ \mathbf{v}'_F = \arg\min_{\mathbf{v}'} J^F_{obs}(I_F, \mathbf{v}', \mathbf{v}'_{F-1}, ..., \mathbf{v}'_C), \end{array} \right. \tag{11}$$

where the finest scale $s = 2^F$ corresponds to the pixel resolution and the coarsest scale is noted $s = 2^C$.

In pratice, equations in (11) are usually solved independently from the coarsest to the finest scales. This approach has the drawback of freezing (*i.e.* leaving unchanged), at a given scale, all the previous coarser estimates. Moreover, the major weakness of this strategy is the arbitrary approximation of the original functional (4) by a set of coarse scale data terms (10), which are defined at different scales by a modification of the original input images with (9) and by a linearization of model (1) around the previous motion estimate.

In the next section, we will see that this multiresolution strategy has a mathematically-sound formulation within the framework of wavelet representations.

3 Fast multiscale motion estimation on wavelet bases

To estimate motion structures of very different sizes minimizing the functional (4), it is necessary to use a proper scale-space representation. The wavelet transform provides a consistent multiresolution representation by motion decomposition on a basis of scale-space atoms.

3.1 Wavelet decomposition of optic flow

Let $\phi \in \mathcal{L}^2(\mathbb{R})$ be a scaling function and let $\psi \in \mathcal{L}^2(\mathbb{R})$ be its associated wavelet. Then, the set of functions

$$\{\phi_k(\mathbf{x}), \psi^1_{j,k}(\mathbf{x}), \psi^2_{j,k}(\mathbf{x}), \psi^3_{j,k}(\mathbf{x})\}, \quad k \in \mathbb{N}^2, j \in \mathbb{N}^+_0, \tag{12}$$

[2] A Gaussian kernel of variance proportional to 2^j is commonly used.

where

$$\left\{\begin{array}{ll} \phi_k(\mathbf{x}) & \triangleq \phi(x_1-k_1)\phi(x_2-k_2), \\ \psi^1_{j,k}(\mathbf{x}) & \triangleq \psi(x_1 2^{-j}-k_1)\phi(x_2 2^{-j}-k_2), \\ \psi^2_{j,k}(\mathbf{x}) & \triangleq \phi(x_1 2^{-j}-k_1)\psi(x_2 2^{-j}-k_2), \\ \psi^3_{j,k}(\mathbf{x}) & \triangleq \psi(x_1 2^{-j}-k_1)\psi(x_2 2^{-j}-k_2), \end{array}\right. \tag{13}$$

forms an orthogonal basis of $\mathcal{L}^2(\mathbb{R}^2)$ [9]. We define the following subsets of $\mathcal{L}^2(\mathbb{R}^2)$:

$$\mathbf{V}_j \triangleq \{f(\mathbf{x}) \in \mathcal{L}^2(\mathbb{R}^2) \mid f(\mathbf{x}) = \sum_k \theta^0_k \phi_k(\mathbf{x}) + \sum_{i=1}^{3}\sum_{l=1}^{j}\sum_k \theta^i_{k,l}\psi^i_{l,k}(\mathbf{x});\ \sum_{i,l,k}(\theta^i_{k,l})^2 < \infty\}. \tag{14}$$

These sets representing approximation space at scale 2^j will prove to be useful in the interpretation of the proposed method in section 4.

We consider the decomposition of the components of the motion vector $\mathbf{v}(\mathbf{x}) = [u(\mathbf{x})\, v(\mathbf{x})]^T$ on basis (12). The projection coefficients of $u(\mathbf{x})$ writes

$$\left\{\begin{array}{ll} (\theta_u)^0_{C,k} = & \langle u(\mathbf{x}), \phi_{C,k}(\mathbf{x})\rangle,\ \ \forall k \in \mathbb{N}^2 \\ (\theta_u)^i_{j,k} = & \langle u(\mathbf{x}), \psi^i_{j,k}(\mathbf{x})\rangle,\ \ \forall k \in \mathbb{N}^2, i \in \{1,2,3\}, j \in [F,C] \subset \mathbb{N}, \end{array}\right. \tag{15}$$

where $\langle\cdot,\cdot\rangle$ denotes the inner product in $\mathcal{L}^2(\mathbb{R})$. Therefore, $u(\mathbf{x})$ can be expressed as

$$u(\mathbf{x}) = \sum_k (\theta_u)^0_{C,k}\phi_{C,k}(\mathbf{x}) + \sum_{j=C}^{F}\sum_{i,k}(\theta_u)^i_{j,k}\psi^i_{j,k}(\mathbf{x}). \tag{16}$$

A similar decomposition can be consider for $v(\mathbf{x})$. These decompositions then lead to two sets of coefficients associated to the two motion components u and v, namely

$$\left\{\begin{array}{l} \mathbf{\Theta}_u = \{((\theta_u)^0_{C,k}, (\theta_u)^i_{j,k})^T | i \in \{1,2,3\},\ j \in [F,C], k \in [0..2^j-1]\} \\ \mathbf{\Theta}_v = \{((\theta_v)^0_{C,k}, (\theta_v)^i_{j,k})^T | i \in \{1,2,3\},\ j \in [F,C], k \in [0..2^j-1]\} \end{array}\right. . \tag{17}$$

We denote by $\mathbf{\Theta} = [\mathbf{\Theta}_u, \mathbf{\Theta}_v]^T$ the set of all coefficients, so that (16) can be rewritten as:

$$\begin{aligned} \mathbf{v}(\mathbf{x}) &= \left[\begin{array}{ccc|ccc} \phi_{C,k}(\mathbf{x}), & \cdots, & \psi^i_{F,k}(\mathbf{x}) & 0, & \cdots, & 0 \\ 0, & \cdots, & 0 & \phi_{C,k}(\mathbf{x}), & \cdots, & \psi^i_{F,k}(\mathbf{x}) \end{array}\right]\mathbf{\Theta}, \\ &= \Phi(\mathbf{x})\mathbf{\Theta}. \end{aligned} \tag{18}$$

3.2 Multiscale estimation of optic flow

In this section, we emphasize that a multiresolution estimation algorithm naturally arises when considering sequential optimizations of wavelet coefficients $\mathbf{\Theta}$. Hereafter, we present two different algorithms which estimate coefficients $\mathbf{\Theta}$ by minimizing functional (4).

3.2.1 Hessian-based algorithm.

An algorithm, based on the calculation of the Hessian of functional (4), has been proposed in [11] to solve this problem with the motion compensate OFC model (2). Using the linear decomposition (18) on $\mathbf{v} = \tilde{\mathbf{v}} + \mathbf{v}'$ yields $\Phi\boldsymbol{\Theta} = \Phi\tilde{\boldsymbol{\Theta}} + \Phi\boldsymbol{\Theta}'$ and:

$$\begin{aligned} J_{obs}(\boldsymbol{\Theta}') &\triangleq J_{obs}(I, \Phi\tilde{\boldsymbol{\Theta}} + \Phi\boldsymbol{\Theta}'), \\ &= \frac{1}{2}\int_{\Omega} (\Phi\boldsymbol{\Theta}')^T g g^T (\Phi\boldsymbol{\Theta}') + 2(I_1(\mathbf{x} + \Phi\tilde{\boldsymbol{\Theta}}) - I_0(\mathbf{x}))(\Phi\boldsymbol{\Theta}')^T g \, d\mathbf{x} \\ &= \frac{1}{2}\boldsymbol{\Theta}'^T A \boldsymbol{\Theta}' - \boldsymbol{\Theta}'^T b, \end{aligned} \tag{19}$$

where:

- $g(\mathbf{x}) = \nabla I_1(\mathbf{x} + \Phi\tilde{\boldsymbol{\Theta}})$, *i.e.* the gradient of the motion compensated image $\tilde{I}_1$;
- $A = \frac{1}{2}\int_{\Omega} \Phi^T(\mathbf{x}) g(\mathbf{x}) g^T(\mathbf{x}) \Phi(\mathbf{x}) d\mathbf{x}$;
- $b = \int_{\Omega} (I_0(\mathbf{x}) - I_1(\mathbf{x} + \Phi\tilde{\boldsymbol{\Theta}})) g(\mathbf{x})^T \Phi(\mathbf{x}) d\mathbf{x}$.

Minimizing the data term in $\boldsymbol{\Theta}'$, we search an increment satisfying $\hat{\boldsymbol{\Theta}}' = \hat{\boldsymbol{\Theta}} - \tilde{\boldsymbol{\Theta}} = \arg\min J_{obs}(\boldsymbol{\Theta}')$. As the energy is quadratic, the minimum of the convex functional linearized around $\tilde{\boldsymbol{\Theta}}$ is reached at the point where gradient vanish. Therefore, the solution reads:

$$\hat{\boldsymbol{\Theta}}' = A^{-1} b \tag{20}$$

However, the algorithm complexity is very high since the Hessian calculation is very demanding: $\mathcal{O}(KN^5)$ for a signal of size $N = 2^{-C}$ and a conjugate mirror filter (associated to the wavelet) of size K. This limits the use of this algorithm to coarse scales $2^F \gg 2^0$ and to wavelets of very limited support.

3.2.2 Fast gradient-based algorithm.

We propose a low-complexity algorithm based on the calculation of the gradient of functional (4) by two independent wavelet transforms. Conversely to the previous algorithm, this one minimizes the original (non-linearized) model $\mathcal{M} = f_d$ defined in (1). More explicitly, since the functional is convex, the minimizer can be simply obtained by cancelation of the functional gradient. Using decomposition (18), the derivative of the DFD data term with respect to vector $\boldsymbol{\Theta}$ reads:

$$\begin{aligned} \frac{\partial J_{obs}(\boldsymbol{\Theta})}{\partial \boldsymbol{\Theta}}^T \mathrm{d}\boldsymbol{\Theta} &\triangleq \lim_{\beta \to 0} \frac{\partial}{\partial \beta} \int_{\Omega} \frac{1}{2}\Big(I_1(\mathbf{x} + \Phi(\mathbf{x})[\boldsymbol{\Theta} + \beta \mathrm{d}\boldsymbol{\Theta}]) - I_0(\mathbf{x})\Big)^2 d\mathbf{x} \\ &= \int_{\Omega} \Big(I_1(\mathbf{x} + \Phi(\mathbf{x})\boldsymbol{\Theta}) - I_0(\mathbf{x})\Big) \nabla I_1^T(\mathbf{x} + \Phi(\mathbf{x})\boldsymbol{\Theta}) \Phi(\mathbf{x}) \mathrm{d}\boldsymbol{\Theta} d\mathbf{x} \end{aligned} \tag{21}$$

and therefore using (15), one gets:

$$\frac{\partial J_{obs}(\mathbf{\Theta})}{\partial \mathbf{\Theta}_u} = \int_\Omega \Big(I_1(\mathbf{x}+\Phi(\mathbf{x})\mathbf{\Theta}) - I_0(\mathbf{x})\Big)\frac{\partial I_1}{\partial x_1}(\mathbf{x}+\Phi(\mathbf{x})\mathbf{\Theta})(\phi_{C,k}(\mathbf{x}),\ \cdots,\ \psi^i_{F,k}(\mathbf{x}))^T d\mathbf{x}$$
$$\frac{\partial J_{obs}(\mathbf{\Theta})}{\partial \mathbf{\Theta}_v} = \int_\Omega \Big(I_1(\mathbf{x}+\Phi(\mathbf{x})\mathbf{\Theta}) - I_0(\mathbf{x})\Big)\frac{\partial I_1}{\partial x_2}(\mathbf{x}+\Phi(\mathbf{x})\mathbf{\Theta})(\phi_{C,k}(\mathbf{x}),\ \cdots,\ \psi^i_{F,k}(\mathbf{x}))^T d\mathbf{x}. \tag{22}$$

As a consequence, components of the cost function gradient are simply the coefficients of the decomposition of $[I_1(\mathbf{x}+\Phi(\mathbf{x})\mathbf{\Theta}) - I_0(\mathbf{x})]\,\frac{\partial I_1}{\partial x_1}(\mathbf{x}+\Phi(\mathbf{x})\mathbf{\Theta})$ and $[I_1(\mathbf{x}+\Phi(\mathbf{x})\mathbf{\Theta}) - I_0(\mathbf{x})]\,\frac{\partial I_1}{\partial x_2}(\mathbf{x}+\Phi(\mathbf{x})\mathbf{\Theta})$ on the wavelet basis. Using a gradient based algorithm, we obtain the minimizer $\hat{\mathbf{\Theta}}$. The complexity of the algorithm is much lower. Suppose that the conjugate mirror filters associated to the wavelet and scaling functions have K non-zero coefficients. Then, a step of the gradient algorithm has the complexity of two fast wavelet transforms of complexity $\mathcal{O}(KN)$ [9].

4 High-order regularization

In order to introduce wavelet-based high-order multiscale regularizers we first need to define the notion of "Lipschitz regularity" and derive accordingly the properties of wavelet coefficients decay.

4.1 Vanishing moments, Lipschitz regularity and coefficient decay

A wavelet $\psi(x) \in \mathcal{L}^2(\mathbb{R})$ has n vanishing moments if :

$$\int_{\mathbb{R}} x^\ell \psi(x) dx = 0, \text{ for } 0 \le \ell < n. \tag{23}$$

Hence a wavelet with n vanishing moments is orthogonal to any polynomial of degree $n-1$.

A function $w(x) \in \mathcal{L}^2(\mathbb{R})$ is said to be uniformly Lipschitz α over Ω if it satisfies:

$$|w(x) - p_\nu(x)| \le K|x-\nu|^\alpha, \quad \forall\, \nu \in \Omega, \forall x \in \mathbb{R}, \tag{24}$$

where $p_\nu(x)$ is a polynomial of degree $m = \lfloor \alpha \rfloor$ and K a constant independent of ν. It can be shown that a function $w(x)$ which is Lipschitz $\alpha > m$ is necessarily m times continuously differentiable (*i.e.* $w(x) \in \mathcal{C}^m(\mathbb{R})$).

The decay of the wavelet coefficients with the scale can be related to the Lipschitz regularity of $w(x)$ and the number of vanishing moments of $\psi(x)$ [9]. In particular, we can distinguish between the two following cases:

- if $w(x)$ is Lipschitz $\alpha > n$, the wavelet coefficients decay as

$$\langle w(x), \psi_{j,k}(x)\rangle \sim 2^{j(n+\frac{1}{2})}. \tag{25}$$

  This result is a direct consequence of the link which exists between wavelet coefficients and the n^{th} derivative of a differentiable function:

$$\lim_{j\to\infty} \frac{\langle w(x), \psi_{j,k}(x)\rangle}{2^{j(n+\frac{1}{2})}} \propto \frac{\partial^n w(x)}{\partial x^n}. \tag{26}$$

Note that an interesting particular case of (26) arises when $w(x)$ is a polynomial of degree $m < n$. In such a case, $\alpha = \infty$ and we also have from (23) that all the wavelet coefficients are equal to zero.

- if $w(x)$ is Lipschitz $\alpha < n$, the wavelet coefficients decays as $\langle w(x), \psi_{j,k}(x)\rangle \sim 2^{j(\alpha+\frac{1}{2})}$. A proof of this result can be found in [7].

These results can be easily extended to the case of two-dimensional signals. In particular, projecting a function $u(\mathbf{x}) \in \mathcal{C}^{2n}(\mathbb{R}^2)$ onto $\psi^i_{j,k}(\mathbf{x})$ is asymptotically equivalent to applying an n^{th}-order oriented derivative operators, *i.e.*

$$\begin{aligned}
\lim_{j\to-\infty} \frac{(\theta_u)^1_{j,k}}{2^{j(n+1)}} &\propto \frac{\partial^n u(\mathbf{x}-k2^{-j})}{\partial x_1^n}, \\
\lim_{j\to-\infty} \frac{(\theta_u)^2_{j,k}}{2^{j(n+1)}} &\propto \frac{\partial^n u(\mathbf{x}-k2^{-j})}{\partial x_2^n}, \\
\lim_{j\to-\infty} \frac{(\theta_u)^3_{j,k}}{2^{j(n+1)}} &\propto \frac{\partial^{2n} u(\mathbf{x}-k2^{-j})}{\partial x_1^n x_2^n},
\end{aligned} \tag{27}$$

where $(\theta_u)^i_{j,k} \triangleq \langle u(\mathbf{x}), \psi^i_{j,k}(\mathbf{x})\rangle$. Therefore, if $u(\mathbf{x})$ has bounded derivatives it follows that

$$|(\theta_u)^i_{j,k}| \sim 2^{j(n+1)} \quad \forall i \in \{1,2,3\}. \tag{28}$$

In particular, (28) holds if $u(\mathbf{x})$ is Lipschitz $\alpha > n$.

Moreover, if $u(\mathbf{x})$ is Lipschitz $\alpha < n$ it can be shown following the same reasoning as in [9] that:

$$|(\theta_u)^i_{j,k}| \sim 2^{j(\alpha+1)}. \tag{29}$$

4.2 High-order optic flow regularization

Let ψ be a mother wavelet with a fast decay and n vanishing moments and let α be the uniform Lipschitz isotrope regularity of motion components u and v.

a) Hard constraints on optic flow regularity. We suppose the considered wavelet has a sufficiently high number of vanishing moments n and assume optic flow is a polynomial function of order $m < n$. Then, (27) implies that wavelet coefficients vanish when scales tend to zero. Therefore, in this case solving the optic flow estimation problem on a wavelet basis with a n^{th} order regularizer:

$$\left\{\begin{array}{l}
\hat{\mathbf{v}} = \Phi\Big(\arg\min_{\boldsymbol{\Theta}} J_{obs}(I, \Phi(\boldsymbol{\Theta}))\Big) \\
\text{s.t. } \forall \mathbf{x} \in \mathbb{R}^2, \;\; \frac{\partial^n u(\mathbf{x})}{\partial x_1^n} = \frac{\partial^n u(\mathbf{x})}{\partial x_2^n} = \frac{\partial^{2n} u(\mathbf{x})}{\partial x_1^n x_2^n} = 0 \\
\qquad\qquad \frac{\partial^n v(\mathbf{x})}{\partial x_1^n} = \frac{\partial^n v(\mathbf{x})}{\partial x_2^n} = \frac{\partial^{2n} v(\mathbf{x})}{\partial x_1^n x_2^n} = 0.
\end{array}\right. \tag{30}$$

This is equivalent to use an explicit regularization scheme, estimating the motion field in an approximation space $\mathbf{V}_L$, where $C \gg L > F$. Thus, it results in estimating optic flow on a truncated wavelet basis, where components at scales

$s \in [2^F, 2^L]$ are omitted. Hence, the solution of (30) is simply obtained by solving the lower-dimensional problem:

$$\begin{cases} \hat{\mathbf{v}}_L = \Phi\Big(\arg\min_{\mathbf{\Theta}} J_{obs}(I, \Phi(\mathbf{\Theta}))\Big) \\ \text{s.t.} \{(\theta_u)^i_{j,k} = (\theta_v)^i_{j,k} = 0, \forall i \in \{1,2,3\}, \forall k \in \mathbb{R}^2, \forall j < L\}. \end{cases} \tag{31}$$

As proposed in the previous section, the minimum of (31) can be simply obtained by canceling the gradients (22). Note, that by varying the number of wavelet vanishing moments, we are able to impose a hard constraint on the n-th order regularity.

b) Multiscale interpolation. The equivalence between (30) and (31) stands only in the limit case of scale $s \in [2^F, 2^L]$ close to zero. Since the pixel resolution is the finest accessible scale, wavelet coefficients at the finest scale 2^F do not necessarily vanish in practice. Moreover, in general the solution may deviate from a polynomial of order m, and is generally only an approximation of a function Lipschitz $\alpha < n$ (see previous section) with $\lfloor \alpha \rfloor = m$. Therefore, instead of imposing wavelet coefficients to vanish in the scale range $[2^F, 2^L]$, we rather propose to prolongate the motion regularity (*i.e.* the wavelet coefficient decay) in this range by multiscale interpolation [9]. Indeed, multiscale interpolation is the orthogonal projection of the solution estimated at scale 2^L on the finest approximation space $\mathbf{V}_F$. For an approximation $\hat{\mathbf{v}}_L$ in the space $\mathbf{V}_L$, the solution $\hat{\mathbf{v}}$ interpolated at scale 2^F reads:

$$\hat{\mathbf{v}} = \sum_{n_1=-\infty}^{+\infty} \sum_{n_2=-\infty}^{+\infty} \hat{\mathbf{v}}_L(n_1 2^F, n_2 2^F) \phi_F\Big(\frac{x_1 - n_1 2^F}{2^F}, \frac{x_2 - n_2 2^F}{2^F}\Big). \tag{32}$$

The interpolation function ϕ_F is defined as the autocorrelation of the orthogonal scaling function: $\phi_F = \phi \star \bar{\phi}$, where $\star$ and $\bar{\phi}$ denote respectively the convolution operator and the complex conjugate of ϕ. The solution being at small scales a polynomial of order $m \leq n$, wavelet coefficients decay in $m+1$ (*i.e.* $\lfloor \alpha \rfloor + 1$). The decay imposed at small scales $[2^F, 2^L]$ therefore constitute an approximated prolongation of the decay in $\alpha + 1$ estimated at coarser scales $[2^L, 2^C]$.

c) Soft constraints on optic flow regularity. Considering now the more general case where the solution is not limited to polynomial function but is Lipschitz $\alpha > n$ (see previous section), we propose to introduce a global n^{th} order regularization functional designed on the properties of wavelet coefficient decay given in (27):

$$\begin{aligned} J_{reg}(\mathbf{\Theta}) &= \frac{1}{2} \int_\Omega \Big(\frac{\partial^n u}{\partial x_1^n}\Big)^2 + \Big(\frac{\partial^n u}{\partial x_2^n}\Big)^2 + \Big(\frac{\partial^{2n} u}{\partial x_1^n x_2^n}\Big)^2 + \Big(\frac{\partial^n v}{\partial x_1^n}\Big)^2 + \Big(\frac{\partial^n v}{\partial x_2^n}\Big)^2 + \Big(\frac{\partial^{2n} v}{\partial x_1^n x_2^n}\Big)^2 d\mathbf{x} \\ &= \frac{1}{2} \sum_{i,j,k} (\beta_j (\theta_u)^i_{j,k})^2 + (\beta_j (\theta_v)^i_{j,k})^2 \end{aligned} \tag{33}$$

where $\beta_j = 2^{-j(n+1)}$ denote multiplicative factors. Note that the order of regularization is simply tuned by varying the number of vanishing moments of

the mother wavelet. The gradient of the regularization functional thus reads:

$$\frac{\partial J_{reg}(\mathbf{\Theta})}{\partial \mathbf{\Theta}} = \begin{pmatrix} \vdots \\ \beta_j(\theta_u)^i_{j,k} \\ \vdots \\ \hline \vdots \\ \beta_j(\theta_v)^i_{j,k} \\ \vdots \end{pmatrix} \tag{34}$$

Assembling the gradients of the data term (21) and the gradient of the n^{th}-order regularizer (34), we obtain the gradient of the global functional (5). A gradient descent algorithm is then used to obtain the minimizer $\hat{\mathbf{\Theta}}$ and therefore achieve multiscale motion estimation. When $\alpha < n$, the proposed regularizer does no longer constitute a n^{th} order regularizer (see previous section). However, it can constitute a good approximation as long as n is not too large. In any case, we can make the regularizer exact since there always exist a wavelet with a sufficiently low number of vanishing moment satisfying $n < \alpha$.

5 Experiments

5.1 Implementation

Daubechies wavelets of variable order have been chosen since they have a minimum support size for a given number of vanishing moments [9]. Input images being finite signals, it is necessary to construct wavelet bases of $\mathcal{L}^2[0,1]$. Thus, the wavelet basis of $\mathcal{L}^2(\mathbb{R})$ is transformed by periodizing each scaling function and wavelet of the basis. In order to handle nicely large displacements [11], wavelet coefficients are sequentially estimated from the coarsest to the finest scales. More precisely, beginning from the estimation of the coarsest approximation in $\mathbf{V}_C$, wavelet basis is refined with details in $\mathbf{V}_{j-1} - \mathbf{V}_j$ at scale 2^j until scale 2^L is reached. At each refinement level, minimization of the cost function is efficiently achieved with a Quasi-Newton gradient algorithm and using Wolf conditions to fix the optimal gradient step (L-BFGS algorithm [10]). The gradient descent is initialized with the estimate obtained at the previous level. This strategy enables the update of the coarser coefficients while estimating details at finer scales.

5.2 Fluid image data sets

Sequences of images depicting fluid flows have been chosen for assessing the methods. Accurate motion estimation on such data remains very challenging. Nevertheless, we show in the following that high-order multiscale optic flow regularizers are well designed for the characterization of fractal motion such as turbulence.

5.2.1 Synthetic turbulence

The first data set used for evaluation is a synthetic sequence of Particle Imagery Velocimetry (PIV) images of 256×256 pixels, representing small particles (of

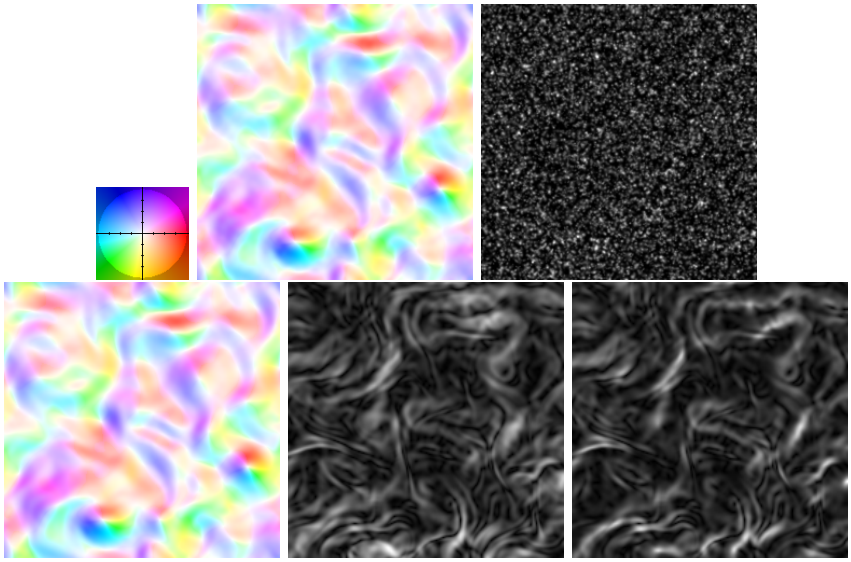

Figure 1: From left to right: Up, color legend [1], ground truth and sample input PIV image. Below, estimated motion (case b of section 4.2), along with associated end point error and Barron error maps. In the visualization of [1] color and intensity respectively code for vector orientation and magnitude.

radius below 4 pixels) advected by a two-dimensional periodic turbulent flow. The dynamic of the fluid flow is given by numerical simulation of 2D Navier-Stokes equations. Since true velocity fields are known, comparisons and errors computation can easily be done. An image of the sequence is displayed in Fig. 1 together with its associated motion ground truth. Estimated velocity fields are evaluated based on the Root Mean Squared end point Error (RMSE) and Mean Barron's angular Error (MBE).

Reg.	Horn& Schunck (1981) first-order [6]	Corpetti& al (2002) div-curl [4]	Yuan& al (2007) div-curl [12]	Heas& al (2009) self-similar [5]	Proposed method 7^{th} order
RMSE	0.13851	0.13402	0.0960	0.0914	0.0905
BME	4.2656	4.3581	3.0458	2.8836	2.8994

Table 1: Comparison of RMSE and BME between state of the art and proposed estimators. Results obtained solving (32) (case b of section 4.2) have been projected onto the null-divergence space [5] to make them consistent with results in [12] [5].

The two hard constraint regularization schemes (cases a and b of section 4.2) have first been evaluated on this sequence. According to the image size of 2^8, scales in the range $[2^0, 2^7]$ have been considered in the dyadic multiresolution representation. An approximation space $\mathbf{V}_L$ corresponding to scale $2^L = 2^5$ was chosen for solving the hard-constraint estimation problems defined in (31) and (32). Motion field estimate obtained with a hard constraint regularization complemented by multiscale interpolation is presented in Fig. 1 together with the end point error and the Barron error maps. As shown in table 1, this high-

order regularization scheme outperforms the best state of the art results in terms of RMSE.

In Fig. 2, the RMSE is plotted versus the number of vanishing moments of the wavelet. It appears that the regularizer based on (32) (case b in section 4.2) is globally slightly better than (31) (case a). Both errors globally decrease when the number of vanishing moments increases, reaching a minimum at 7 vanishing moments then slightly increasing before stabilizing. Error decrease rate is much slower when the number of vanishing moments is above 3. In order to check the consistency with the theoretical decays, the statistical average of the absolute value of wavelet coefficients w.r.t to scales (so-called first-order structure function) has been computed for the ground truth and motion estimates obtained for varying vanishing moments. Fig. 2 is a log-log plot of the coefficient first-order structure function, computed on the true velocity field. When the number of vanishing moments is greater or equal to the field's Lipschitz regularity ($\alpha \leq n$), coefficients decay slope is bounded by $\alpha + 1$, which is clearly seen on Fig. 2. A similar decay behavior can be observed in Fig. 2 for the structure function of the estimated velocity field.

The soft constraint high-order regularization of (33) (see case c of section 4.2), was then assessed on the same image sequence. The motion field and the associated error maps are displayed in Fig. 3. It can be noticed that non-resolved structures appear to be smaller than on errors maps of Fig. 1. A RMSE of 0.10 and a BME of 3.20 is obtained using a Daubechies wavelet with 3 vanishing moments. Nevertheless, the soft constraint regularization scheme gives slightly better results, when compared to the accuracy obtained with hard-constraint regularization of the finest scale (*i.e.* $2^L = 2^1$) using the same mother wavelet.

5.2.2 Real LIDAR image sequence of atmospheric motion

The second data set used for evaluation consists in eye-safe aerosol "Light Detection and Ranging" (LIDAR) image sequence. We processed a sequence of 25 images of size 602×602 pixels representing scans of an horizontal plane depicting atmospheric motion in the boundary layer. Two consecutive scans separated by 17.3 seconds are visible in Fig. 4. The same figure shows the associated motion estimates, which were obtained using the regularizer and a number of vanishing moments yielding the best results on the PIV image sequence. Results are in good agreement with the visual inspection of the images sequence. A qualitative evaluation was also performed using punctual in-situ ground truth measurements from a micro-meteorogical tower located within the LIDAR scan plane. Motion has been estimated in a window of size 256×256 pixels centered on the measurement tower. Comparison at the tower location between the true and the estimated velocity vector is displayed in Fig. 5. A RMSE of 0.95 pixels calculated for the whole image sequence was obtained with the proposed wavelet based regularizer, which appears to outperform the RMSE of 1.13 pixels obtained with the "div-curl" estimator of [4].

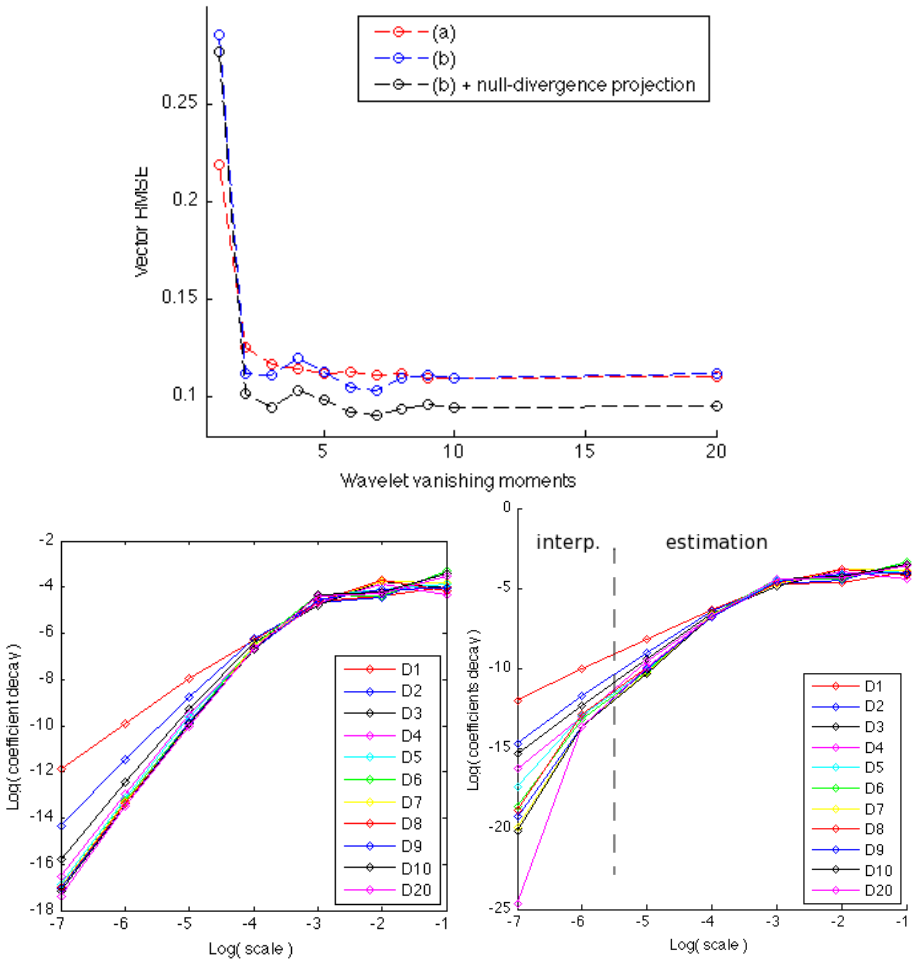

Figure 2: **Up:** RMSE versus wavelet's number of vanishing moments for hard constraint regularizer a and b (see section 4.2). The case b projected onto the null-divergence space [5] is plotted for comparison. **Down:** Log-log plot of first-order structure function of wavelet coefficient associated to the true (left) and the estimated (right) motion field. The estimate was obtained with the high-order regularizer of (32) (see case b in section 4.2) using Daubechies wavelets (D_n) with varying number of vanishing moments n. The slope between scales 2^0 and 2^5 (rightmost part) indicates the field Lipschitz regularity. The slope between scales 2^6 and 2^7 indicates a regularity induced by wavelet interpolation.

6 Conclusion

In this paper, we considered the motion estimation problem from a wavelet-expansion perpective. In particular, we constrained the velocity field to have a proper decomposition onto an wavelet orthogonal basis. The proposed approach was shown to offer a nice mathematical framework for the derivation of effective multiresolution estimation algorithms. In particular, we devised an

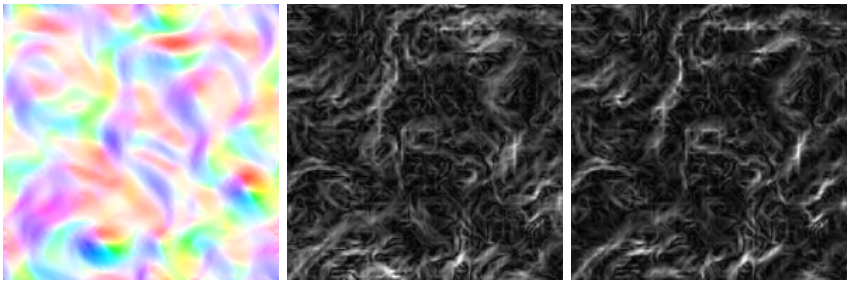

Figure 3: From left to right: Estimated motion with a high-order soft constraint regularization scheme (case c of section 4.2) and associated end point error and Barron error maps.

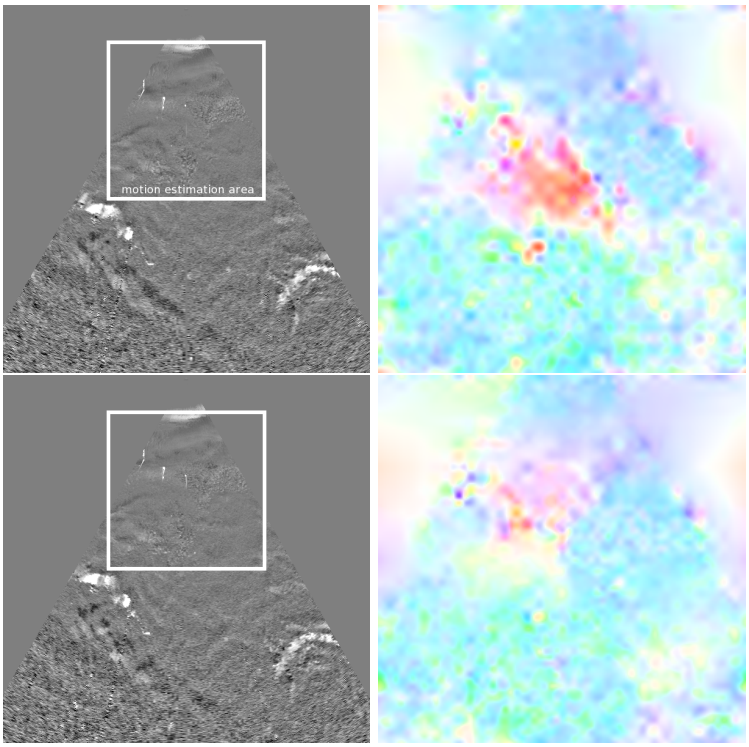

Figure 4: Example of input lidar data frames showing the estimation window and associated color representation of the estimated velocity fields.

iterative estimation procedure having a linear complexity order and exhibiting very good performance. The proposed multiresolution framework was finally shown to be well-suited to the design of high-order regularizers. In particular, three possible implementations of such regularizers were proposed and tested on difficult turbulent-fluid image sequences. The simulations proved the clear superiority of the proposed approach over state-of-the-art methods.

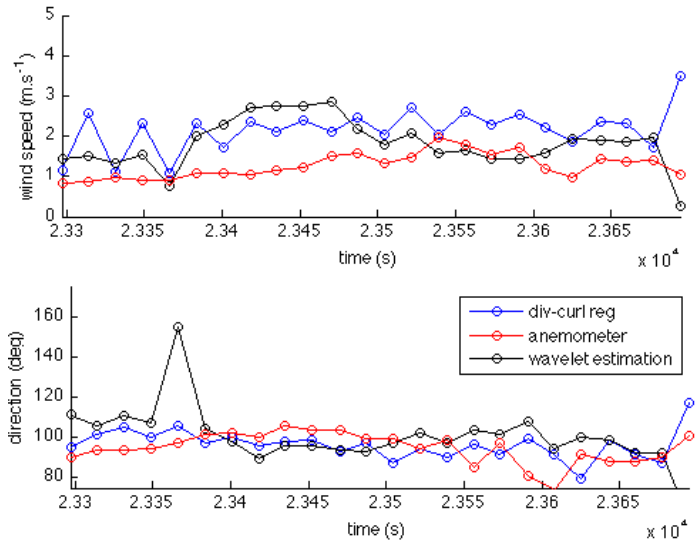

Figure 5: Time comparison of estimated wind speed (left) and direction (right) obtained with the div-curl regularizer of [4] (in blue) and our method with Daubechies mother wavelet (with 3 vanishing moments) (in black), along with in-situ anemometer measurements (in red).

References

[1] S. Baker, D. Scharstein, J.P. Lewis, S. Roth, M. Black, and R. Szeliski. A database and evaluation methodology for optical flow. In *Int. Conf. on Comp. Vis., ICCV 2007*, 2007.

[2] J.R. Bergen, P.J. Burt, R. Hingorani, and S. Peleg. A 3-frame algorithm for estimating two-component image motion. *IEEE Trans. Pattern Anal. Mach. Intell.*, 14(9):886–895, September 1992.

[3] M. Black and P. Anandan. The robust estimation of multiple motions: Parametric and piecewise-smooth flow fields. *Computer Vision and Image Understanding*, 63(1):75–104, 1996.

[4] T. Corpetti, E. Mémin, and P. Pérez. Dense estimation of fluid flows. *Pattern Anal Mach Intel*, 24(3):365–380, 2002.

[5] P. Heas, E. Memin, D. Heitz, and P.D. Mininni. Bayesian selection of scaling laws for motion modeling in images. In *International Conference on Computer Vision (ICCV'09)*, Kyoto, Japan, October 2009.

[6] B. Horn and B. Schunck. Determining optical flow. *Artificial Intelligence*, 17:185–203, 1981.

[7] S. Jaffard. Pointwise smoothness, two-microlocalization and wavelet coefficients. *Publ. Mat.*, page 155–168, 1991.

[8] T. Liu and L. Shen. Fluid flow and optical flow. *Journal of Fluid Mechanics*, 614:253, October 2008.

[9] S. Mallat. *A wavelet tour of signal processing.* Academic Press, 1998.

[10] Jorge Nocedal and Stephen J. Wright. *Numerical Optimization.* Springer Series in Operations Research. Springer-Verlag, New York, NY, 1999.

[11] Y. Wu, T. Kanade, C. Li, and J. Cohn. Image registration using wavelet-based motion model. *Int. J. Computer Vision*, 38(2):129–152, 2000.

[12] J. Yuan, C. Schnoerr, and E. Memin. Discrete orthogonal decomposition and variational fluid flow estimation. *Journ. of Math. Imaging & Vison*, 28:67–80, 2007.

Contents

Centre de recherche INRIA Rennes – Bretagne Atlantique
IRISA, Campus universitaire de Beaulieu - 35042 Rennes Cedex (France)

Centre de recherche INRIA Bordeaux – Sud Ouest : Domaine Universitaire - 351, cours de la Libération - 33405 Talence Cedex
Centre de recherche INRIA Grenoble – Rhône-Alpes : 655, avenue de l'Europe - 38334 Montbonnot Saint-Ismier
Centre de recherche INRIA Lille – Nord Europe : Parc Scientifique de la Haute Borne - 40, avenue Halley - 59650 Villeneuve d'Ascq
Centre de recherche INRIA Nancy – Grand Est : LORIA, Technopôle de Nancy-Brabois - Campus scientifique
615, rue du Jardin Botanique - BP 101 - 54602 Villers-lès-Nancy Cedex
Centre de recherche INRIA Paris – Rocquencourt : Domaine de Voluceau - Rocquencourt - BP 105 - 78153 Le Chesnay Cedex
Centre de recherche INRIA Saclay – Île-de-France : Parc Orsay Université - ZAC des Vignes : 4, rue Jacques Monod - 91893 Orsay Cedex
Centre de recherche INRIA Sophia Antipolis – Méditerranée : 2004, route des Lucioles - BP 93 - 06902 Sophia Antipolis Cedex

Éditeur
INRIA - Domaine de Voluceau - Rocquencourt, BP 105 - 78153 Le Chesnay Cedex (France)
http://www.inria.fr
ISSN 0249-6399